Supplementary Information for

Mechanistic Insight into Oxygen Atom Transfer Reactions by Mononuclear Manganese(IV)-oxo Adducts

Priya Singh,[a] Eleanor Stewart-Jones,[a] Melissa C. Denler,[a] and Timothy A. Jackson*[a]

[a] *The University of Kansas, Department of Chemistry and Center for Environmentally Beneficial Catalysis, 1567 Irving Hill Road, Lawrence, KS 66045, USA.*

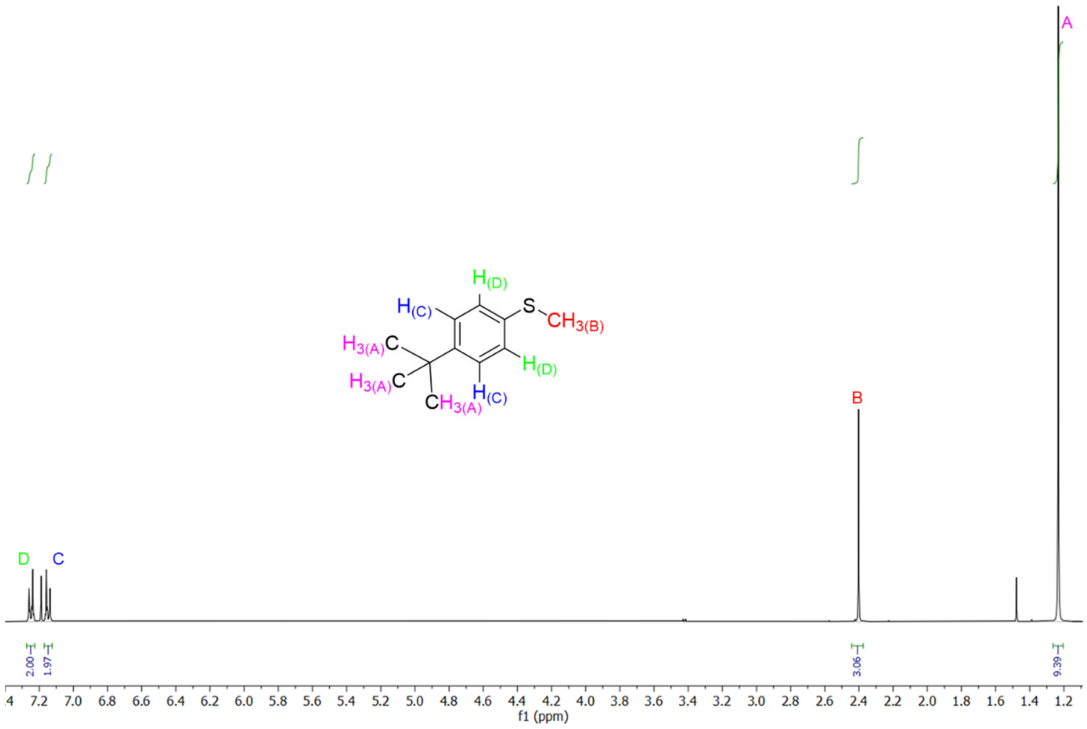

Figure S1. ^{1}H NMR spectrum of *p*-^{tert}butylthioanisole in $CDCl_3$ at 25 °C.

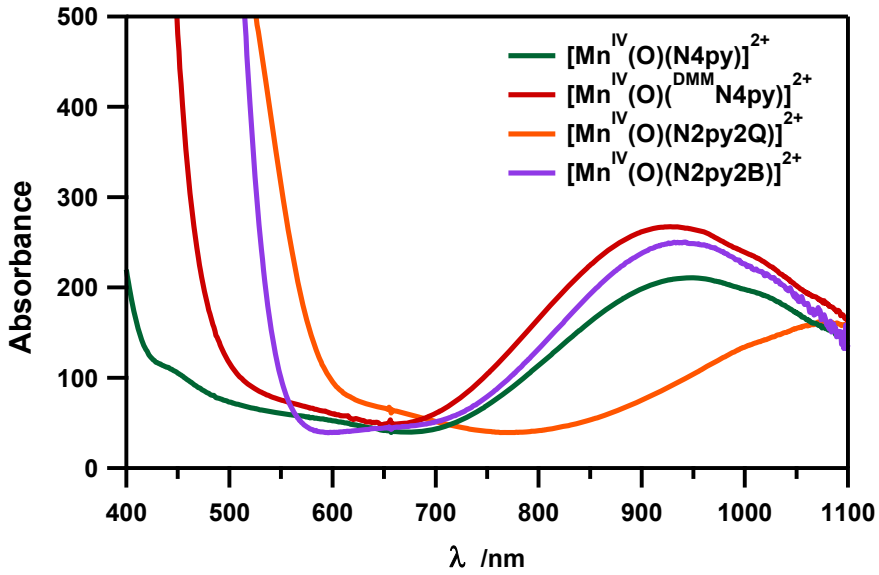

Figure S2. UV-Vis spectra of 1.0 mM Mn^{IV}-oxo complexes $[Mn^{IV}(O)(N4py)]^{+2}$ (**1**), $[Mn^{IV}(O)(2pyN2Q)]^{2+}$ (**2**), $[Mn^{IV}(O)(^{DMM}N4py)]^{2+}$ (**3**) and $[Mn^{IV}(O)(2pyN2B)]^{2+}$ (**4**) in CF_3CH_2OH at 25 °C.

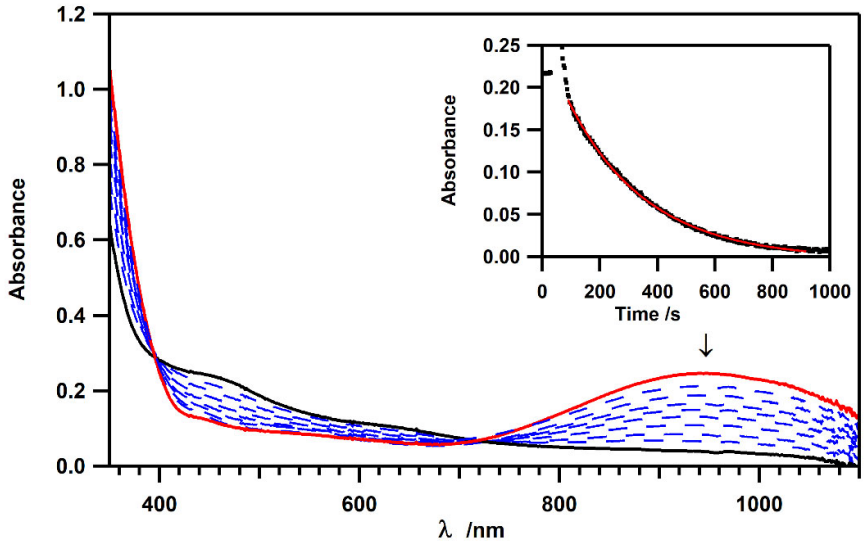

Figure S3. Electronic absorption spectra showing the decay of $[Mn^{IV}(O)(N4py)]^{2+}$ upon addition of 40 equiv. thioanisole. The inset shows the decay of the near-IR signal at 950 nm over time (black dots) and a fit using a pseudo first-order kinetic model (red trace).

Table S1. Summary of the conditions for thioanisole sulfoxidation by Mn^{IV}-oxo adducts **1-4** for the variable-temperature kinetic studies.

	$[Mn^{IV}(O)(N2py2Q)]^{2+}$ (2)	**$[Mn^{IV}(O)(N4py)]^{2+}$ (1)**	**$[Mn^{IV}(O)(^{DMM}N4py)]^{2+}$ (3)**	**$[Mn^{IV}(O)(N2py2B)]^{2+}$ (4)**
Concentration (mM)	1.0	1.0	1.0	1.0
Equiv. PhIO	10	2.5	1.2	2.5
Temperature range (ºC)	-15-15	3-35	35-65	15-45

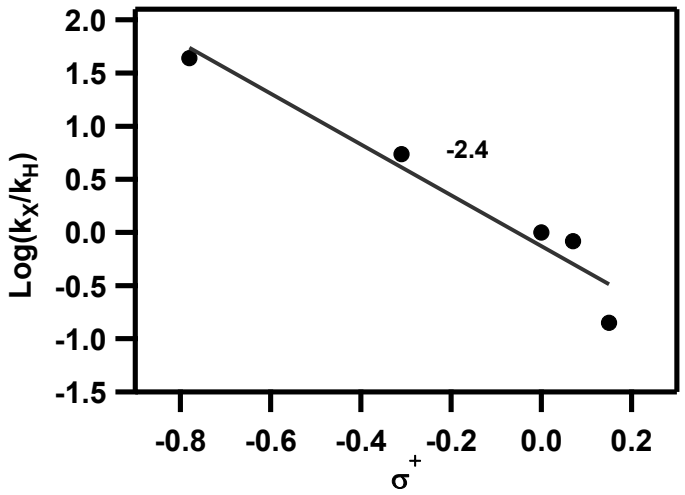

Figure S4. Hammett plot of log(k_X/k_H) against σ^+ of para-X-thioanisole derivatives by **1** at 273 K. Data taken from *J. Am. Chem. Soc*. **2013**, 135, 6388. The original analysis of these data employed the σ value, which yields a better fit. Here we have used σ^+ to provide an even comparison to the data in Figure 4 of the main text.

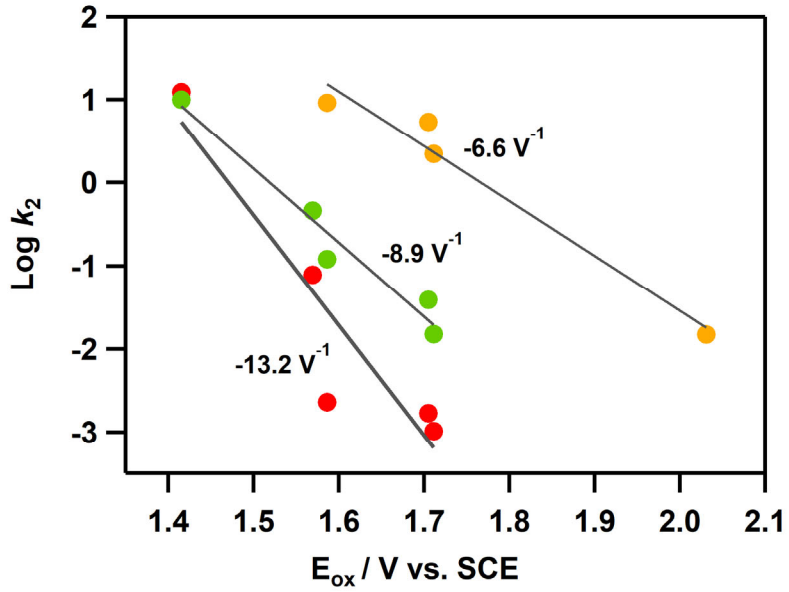

Figure S5. Plot of log k_2 against one-electron oxidation potentials (E_{ox}) of p-X-thioanisole derivatives for **1** (green), **2** (orange) and **3** (red) in CF_3CH_2OH at 298 K. While the data shown for **3** follow the general trend of increasing rate with decreasing E_{ox}, the poorer agreement between the linear fit line and the data points shows that this trend is less linear than the trends for complexes **1** and **2**.

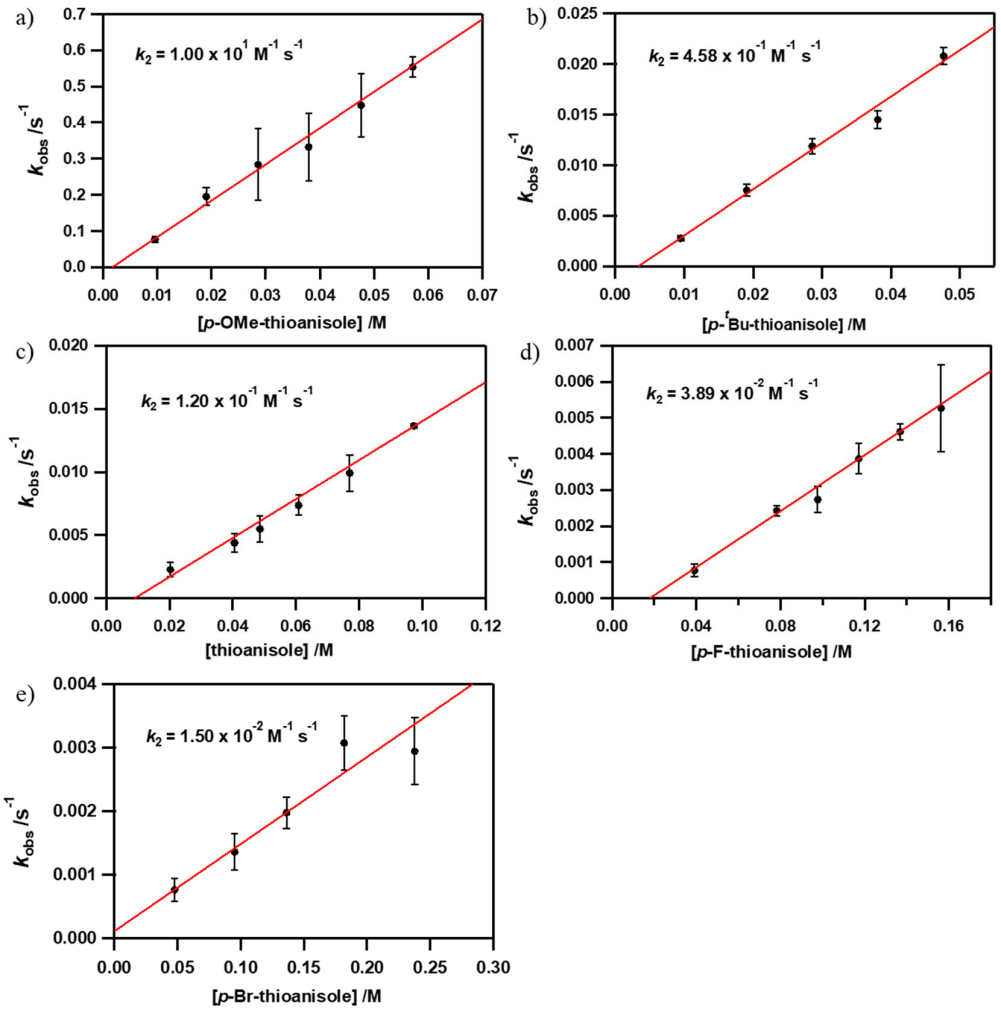

Figure S6. Plots of pseudo-first-order rate constants (k_{obs}) against substrate concentrations to obtain second order rate constants (k_2) for sulfoxidation of a) *p*-methoxythioanisole, b) *p*-^{t}butylthioanisole, c) thioanisole, d) *p*-fluorothioanisole and e) *p*-bromothioanisole by 1 mM solution of **1** in CF_3CH_2OH at 298 K.

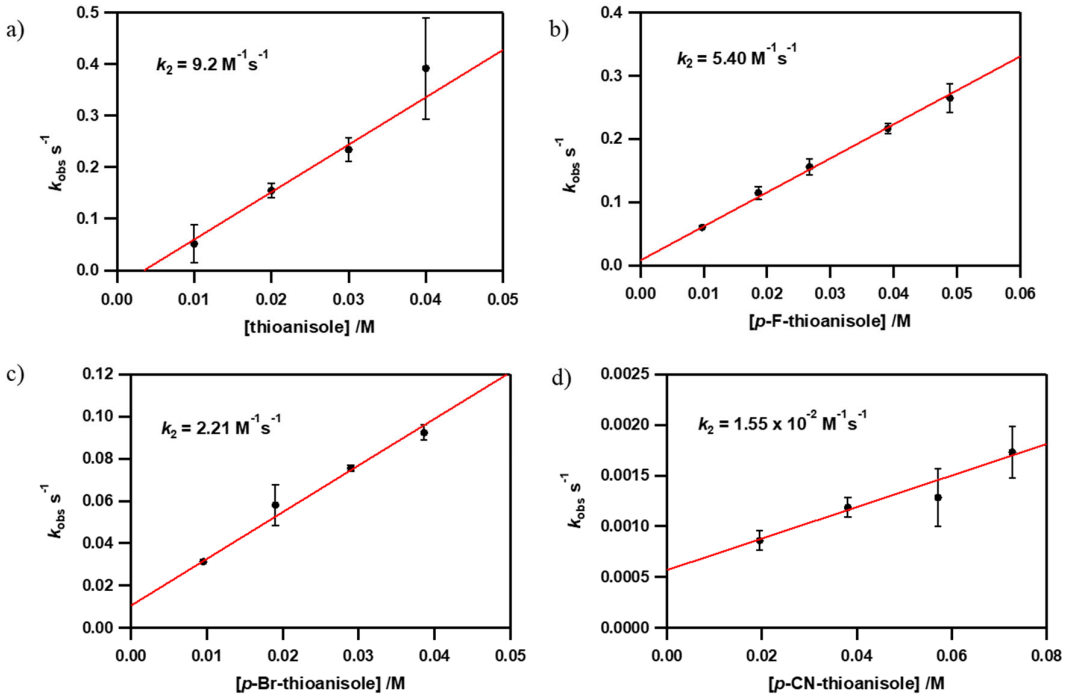

Figure S7. Plots of pseudo-first-order rate constants (k_{obs}) against substrate concentrations to obtain second order rate constant (k_2) for sulfoxidation of a) thioanisole, b) *p*-fluorothioanisole, c) *p*-bromothioanisole and d) *p*-cyanothioanisole, by 1 mM solution of **2** in CF_3CH_2OH at 298 K.

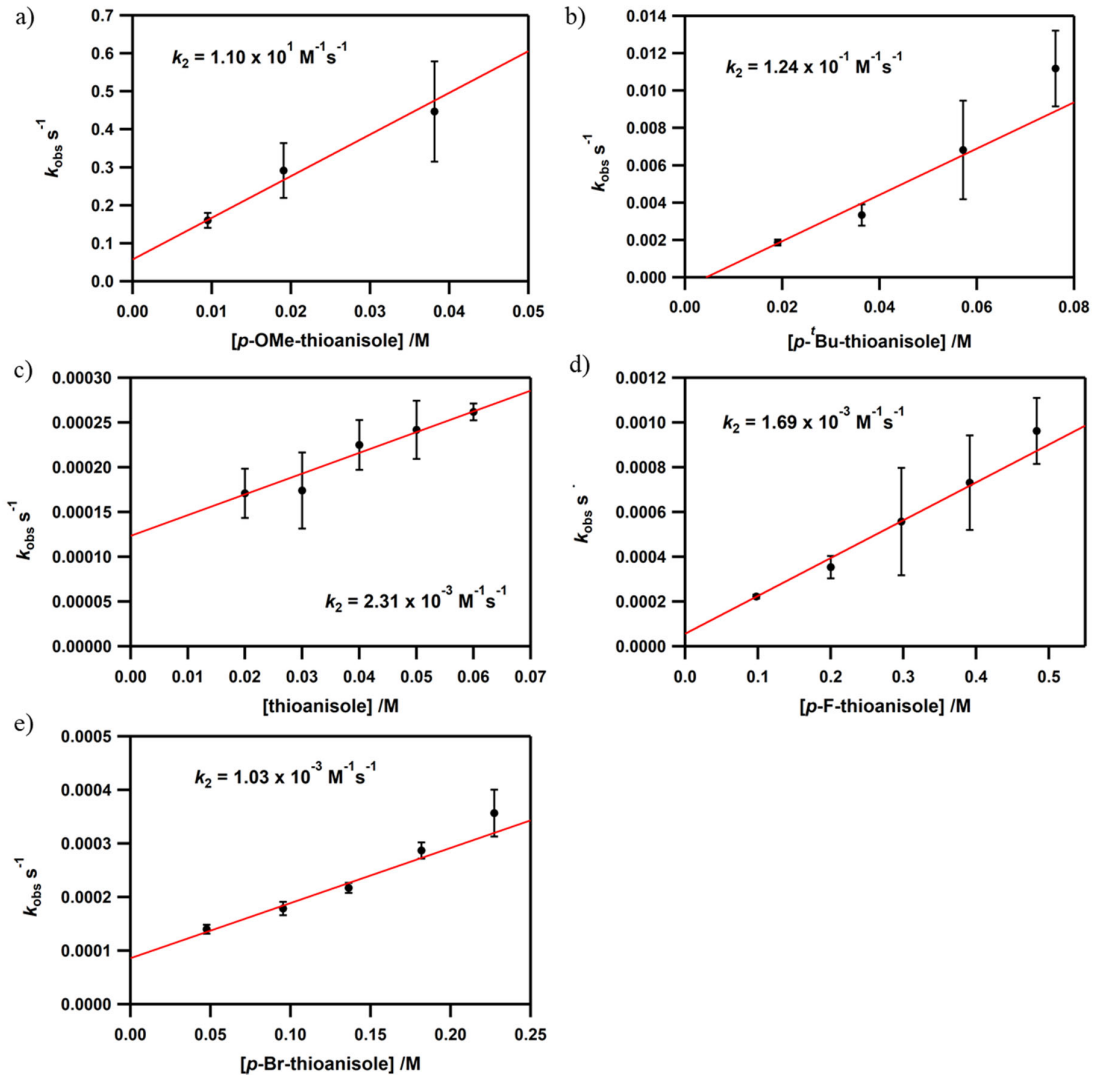

Figure S8. Plots of pseudo-fisrt-order rate constants (k_{obs}) against substrate concentrations to obtain second order rate constant (k_2) for sulfoxidation of a) *p*-methoxythioanisole, b) *p*-^{t}butylthioanisole, c) thioanisole, d) *p*-fluorothioanisole and e) *p*-bromothioanisole by 1mM solution of **3** in CF_3CH_2OH at 298 K.

Kinetic experiments with complex $[Mn^{IV}(O)(N2py2B)]^{2+}$ (4).

Formation of 4 was achieved by addition of 2.5 equiv. PhIO to a solution of $[Mn^{II}(OH_2)(N2py2B)]^{2+}$ in TFE (trifluoroethyl alcohol) at 298 K. The characteristic near-IR feature at 940 nm decayed upon addition of excess *p*-thioanisole derivatives. The decay rate of this complex could only be fit with pseudo-first order model for the oxidation reactions with *p-tert*-butylthioanisole and thioanisole, and second-order rate constants could be obtained as shown in Figure S10. The plot for *p-tert*-butylthioanisole (Figure S10) shows a large, negative intercept, which indicates some problems with the fit. Any attempts to assess the reactivity of 4 with with *p*-methoxy-thioanisole resulted in kinetics that were too fast to yield reliable rates using a conventional UV-vis spectrometer. With *p*-fluorothioanisole, the kinetics showed a fast initial decay followed by a slower decay phase, implying a complex reaction. Decay kinetics involving the p-bromothioanisole derivative could not be fit to three half-lives (Figure S9).

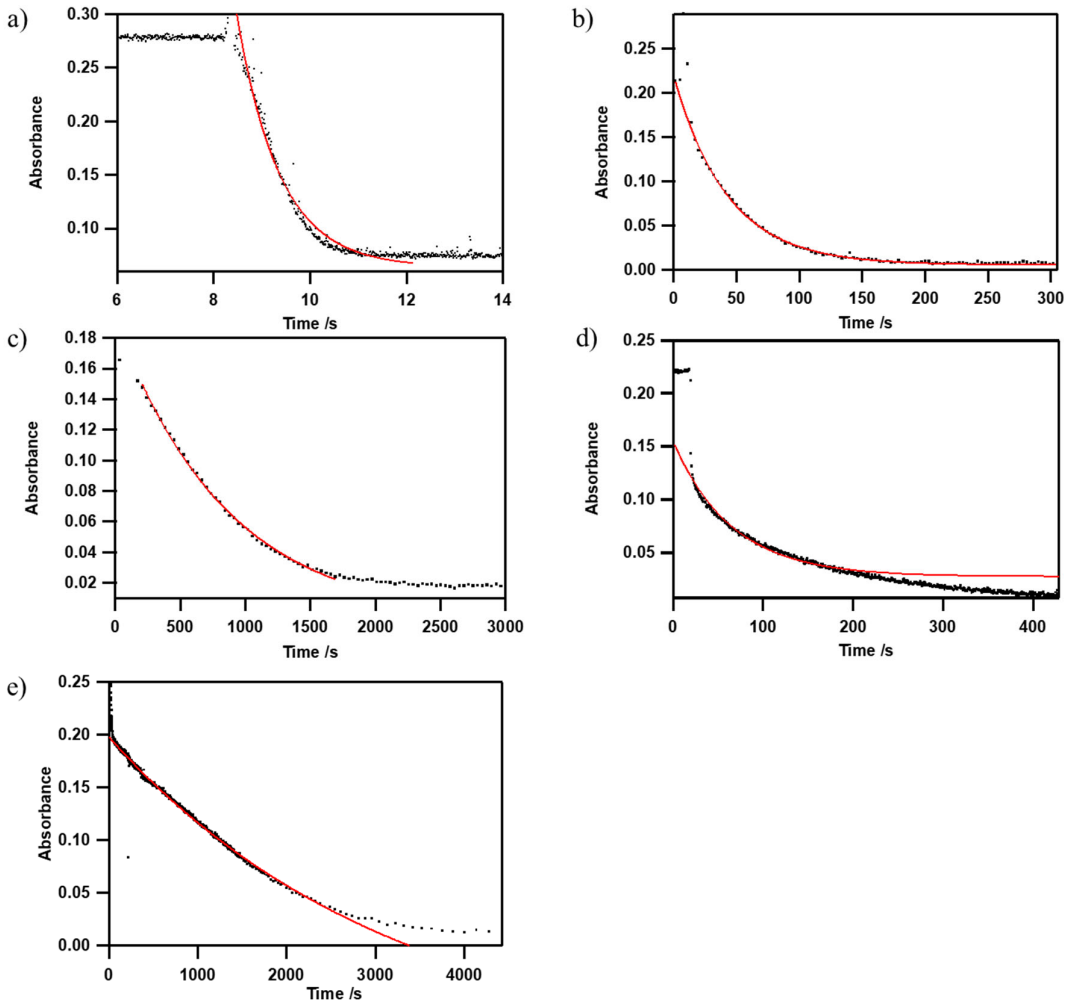

Figure S9. Pseudo-first order fits for the reactions of a) *p*-methoxythioanisole, b) *p*-^{t}butylthioanisole, c) thioanisole, d) *p*-fluorothioanisole and e) *p*-bromothioanisole derivatives with 1 mM solution of **4** in CF_3CH_2OH at 298 K. The poor fits for some of these substrates led to their exclusion from our analysis.

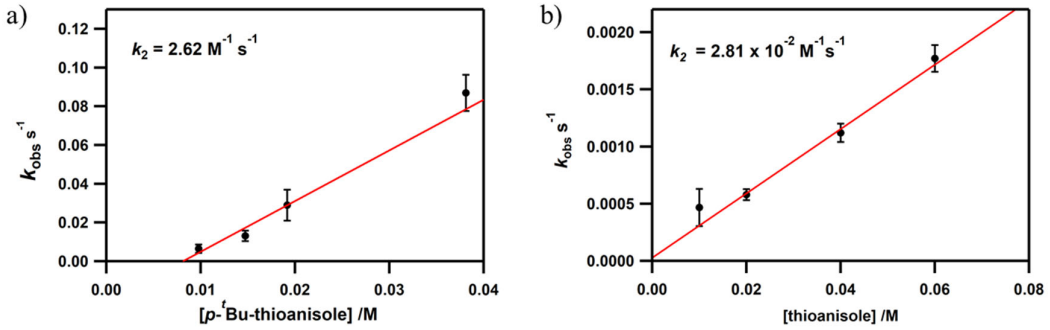

Figure S10. Plots of pseudo-first-order rate constants (k_{obs}) against substrate concentrations to obtain second order rate constant (k_2) for sulfoxidation of a) *p*-^{t}butylthioanisole and b) thioanisole by 1 mM solution of **4** in CF_3CH_2OH at 298 K.

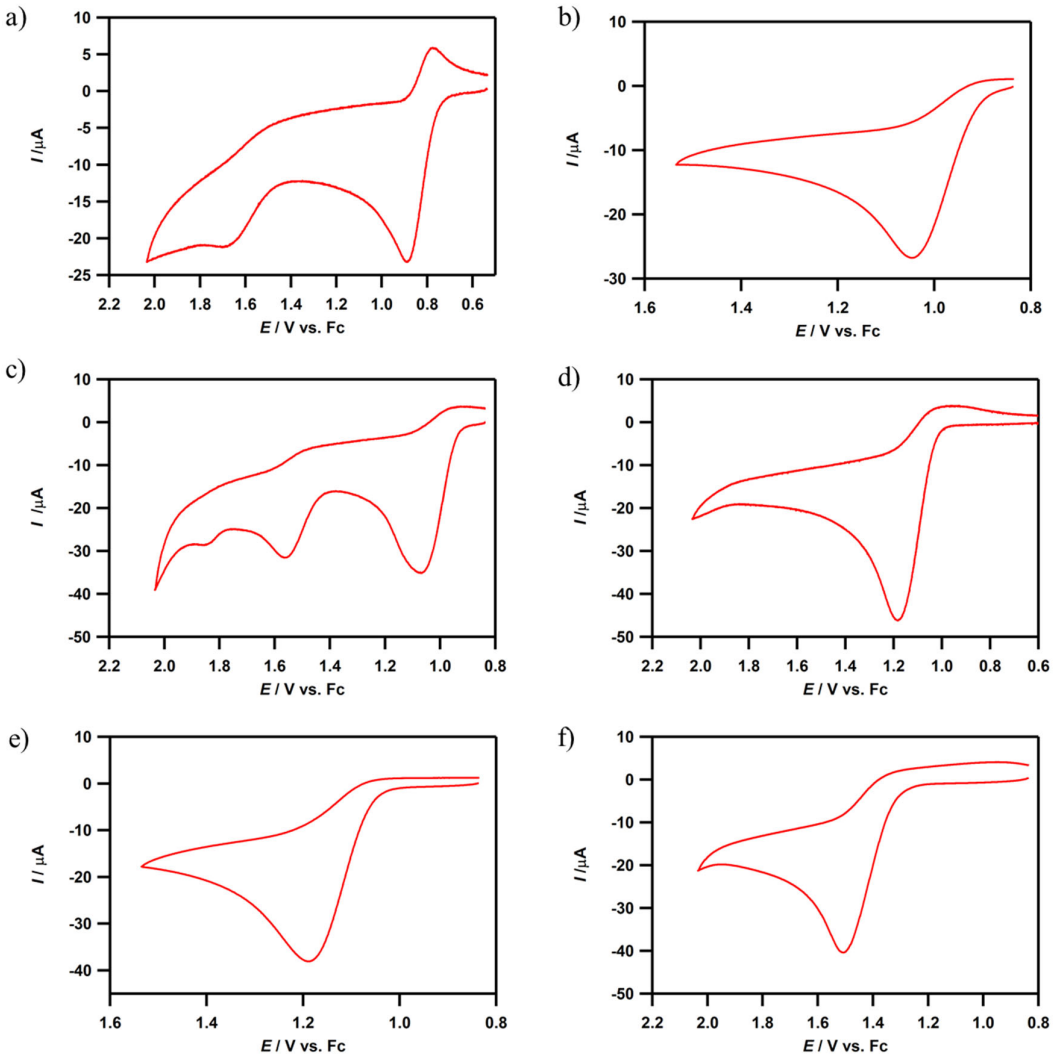

Figure S11. Cyclic voltammograms of a) *p*-methoxythioanisole, b) *p*-^{t}butylthioanisole, c) thioanisole, d) *p*-fluorothioanisole, e) *p*-bromothioanisole and f) *p*-cyanothioanisole recorded in CF_3CH_2-OH with 0.1 M Bu_4NPF_6 electrolyte solution at 100 mV s^{-1} at 298 K.

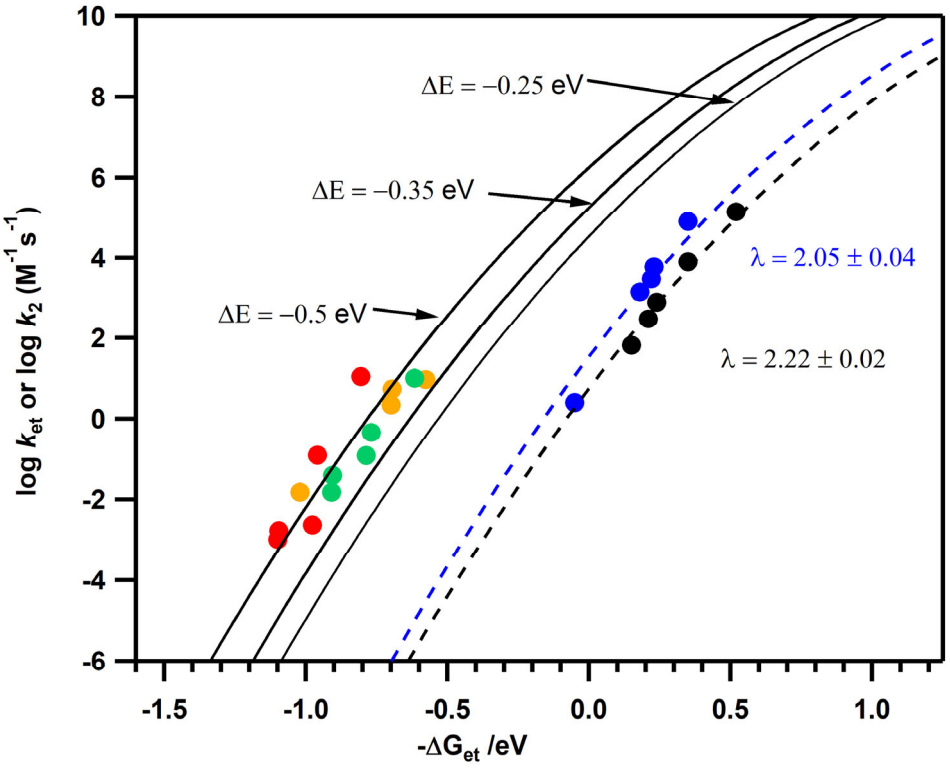

Figure S12. Plot of log k_2 for sulfoxidation of para thioanisole derivatives vs driving force of electron transfer [$-\Delta G_{et} = e(E_{red}-E_{ox})$] from thioanisoles to $[Mn^{IV}(O)N4py]^{2+}$ (green dots), $[Mn^{IV}(O)2pyN2Q]^{2+}$ (orange dots), and $[Mn^{IV}(O)^{DMM}N4py]^{2+}$ (red dots) at 298 K, and $[Mn^{IV}(O)N4py]^{2+}$ in presence of HOTf (blue dots) at 273 K. Black dots represents the driving force dependence of the rate constants (log k_{et}) of the ET from one-electron reductants to $[Mn^{IV}(O)N4py]^{2+}$ at 273 K. The solid black curves represent fits where the reorganization energy has been set at 2.0 eV (similar to the reorganization energy for outer-sphere electron transfer for **1**) and we have then evaluated the effects of uniform shifts in substrate E_{ox} values (ΔE in the figure). Only when ΔE > 350 mV does the fitted curve begin to overlap with the data points. This results reveals a fairly low sensitivity of k_{et} on E_{ox}. Data for the blue and black dots are taken from J. Chen, H. Yoon, Y.-M. Lee, M. S. Seo, R. Sarangi, S. Fukuzumi and W. Nam, Chemical Science, 2015, **6**, 3624-3632.